Analysis of similar event clusters in aftershocks of the 1994 Northridge, California, earthquake

Peter M. Shearer and Jeanne L. Hardebeck
Institute of Geophysics and Planetary Physics, Scripps Institution of Oceanography, University of California, San Diego, La Jolla, California, USA

Luciana Astiz
CTBTO, Vienna, Austria

Keith B. Richards-Dinger
United States Geological Survey, Menlo Park, California, USA

Received 26 June 2001; revised 14 March 2002; accepted 30 May 2002; published 22 January 2003.

[1] We perform waveform cross-correlation on over 14,000 aftershocks of the 1994 Northridge M_W 6.7 earthquake in southern California as recorded by short-period stations of the Southern California Seismic Network (SCSN). Approximately 10–30% of the events belong to similar event clusters, depending upon the similarity criteria that are applied. We relocate events within 218 of these clusters to a relative location accuracy of about 30 m using the differential times obtained from the cross-correlation. These relocated event clusters often show planar features suggestive of faults at depth, and we apply principal parameter analysis to characterize the shape of each cluster and to compute best fitting planes. In several cases, these planes are parallel to the main shock fault plane; however, more generally, the seismicity planes exhibit a wide range of orientations, suggesting complexity in the aftershock faulting. Composite focal mechanisms can be obtained for each cluster by combining the *P* polarity data from individual events. A comparison of polarity measurement differences within similar event clusters provides constraints on the error rate in the individual focal mechanisms. For some clusters, we are able to resolve the primary versus auxiliary fault plane ambiguity by comparing the computed focal mechanisms with the best fitting seismicity planes. Individual event focal mechanisms are in general agreement with the composite focal mechanisms for the similar event clusters. Events occurring along the main shock rupture plane are mainly thrust, whereas events in the hanging wall are predominately strike-slip. *INDEX TERMS:* 7230 Seismology: Seismicity and seismotectonics; 7215 Seismology: Earthquake parameters; 7299 Seismology: General or miscellaneous; *KEYWORDS:* Northridge earthquake, similar event clusters

Citation: Shearer, P. M., J. L. Hardebeck, L. Astiz, and K. B. Richards-Dinger, Analysis of similar event clusters in aftershocks of the 1994 Northridge, California, earthquake, *J. Geophys. Res.*, *108*(B1), 2035, doi:10.1029/2001JB000685, 2003.

1. Introduction

[2] The 1994 Northridge, California, M_W 6.7 earthquake underscored the hazard that thrust faults pose to the Los Angeles region. Identifying and mapping these faults is a challenging problem because the faults often do not extend to the surface. Although reflection seismic techniques may reveal fault structures in the shallow crust [e.g., *Shaw and Suppe*, 1996; *Shaw and Shearer*, 1999], these data generally do not penetrate to depths where large earthquakes nucleate. Background seismicity in the Los Angeles basin occurs at a low rate and is widely scattered, without obvious alignments that would indicate events are occurring on the same fault [e.g., *Hauksson*, 1990, 2000]. Most recent earthquakes near Los Angeles occur as part of aftershock sequences following isolated large events. These aftershock sequences are valuable both for helping constrain the main shock rupture surface and for the clues they may provide regarding the position and orientation of other faults in the region. The Northridge aftershock sequence has been particularly well studied; events have been relocated with custom 1-D velocity models [*Hauksson et al.*, 1995] and 3-D tomographic models [*Mori et al.*, 1995; *Zhoa and Kanamori*, 1995; *Pujol*, 1996; *Hauksson and Haase*, 1997] and event focal mechanisms computed using P wave first motions [*Hauksson et al.*, 1995] and waveform inversions [*Thio and Kanamori*, 1996; *Song and Helmberger*, 1997; *Venkataraman et al.*, 2000].

[3] Figure 1 shows the locations of the 1994 Northridge main shock and its aftershock sequence, together with

0148-0227/03/2001JB000685$09.00

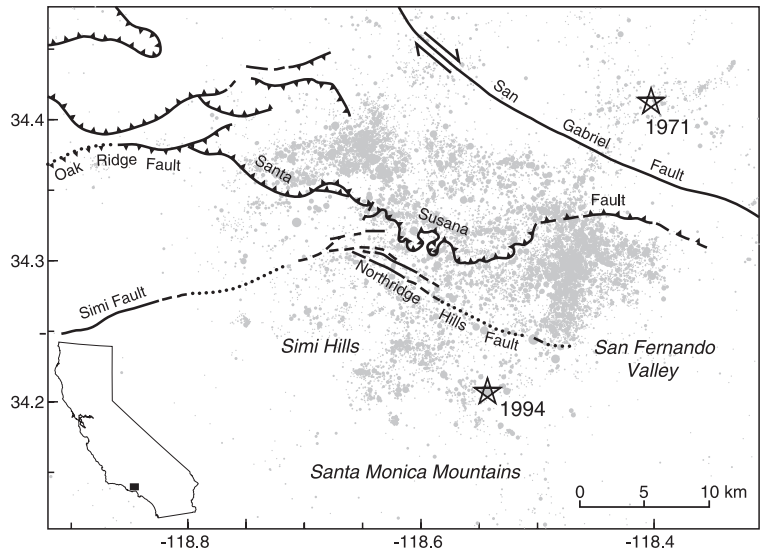

Figure 1. Locations of small earthquakes from 1981 to 1997 (mainly Northridge aftershocks) are shown in gray and compared to mapped surface faults and late Cenozoic contractional structures (adapted from *Unruh et al.* [1997]). The epicenters of the 1971 San Fernando and 1994 Northridge earthquakes are also plotted.

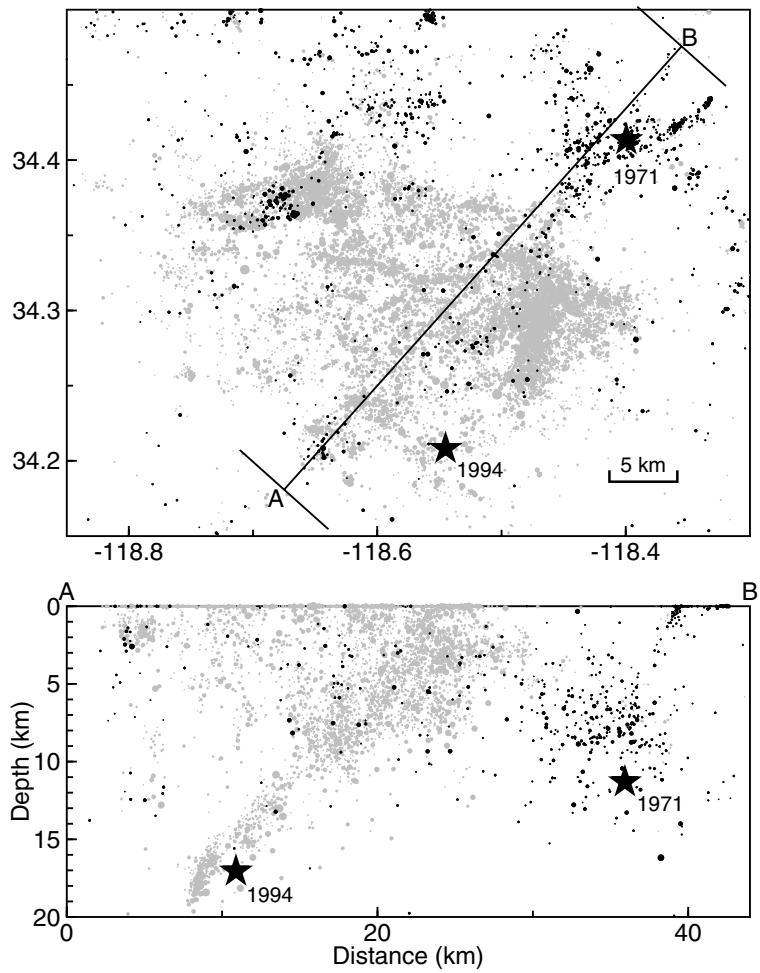

Figure 2. Seismicity in the Northridge area from 1975 to 1998 as located by *Richards-Dinger and Shearer* [2000]. A total of ~15,000 events are plotted. Events prior to the 17 January 1994, Northridge main shock (M_W 6.7) are shown in black; most of these events are late aftershocks of the 1971 San Fernando earthquake. Symbol sizes scale with event magnitude. The main shock locations are shown as stars.

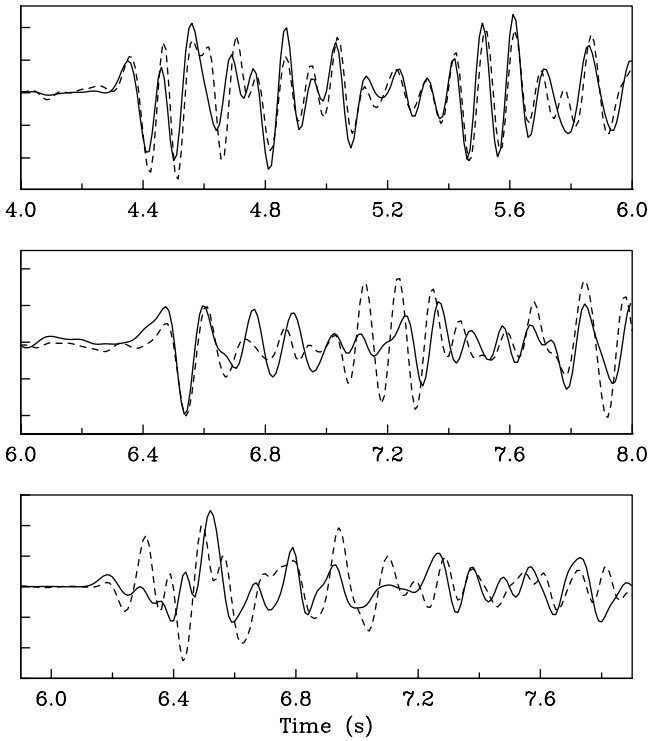

Figure 3. Examples of waveform similarity for computed correlation coefficients of 0.81 (top), 0.62 (middle) and 0.49 (bottom). Data from from stations GFP, JNH and IR2, respectively, from events 3143828 and 3156874 (SCSN ''cusp'' ID numbers).

mapped surface faults (adapted from *Yeats* [1987], *Yeats et al.* [1994], and *Unruh et al.* [1997]). The earthquake occurred on a southward-dipping blind thrust fault, termed the ''Northridge Thrust'' by *Huftile and Yeats* [1996], on which the rupture did not extend to the surface where it could be associated with any previously mapped features. The northward-dipping Santa Susana Fault has no direct relation to the Northridge Thrust although it does appear to have some influence on the distribution of aftershocks [*Hauksson et al.*, 1995]. Figure 2 shows a map view and cross-section of this sequence as relocated using the source-specific station term (SSST) method of *Richards-Dinger and Shearer* [2000]. Northridge aftershocks are shown in gray; prior events are in black. Most of the prior events are late aftershocks of the 1971 San Fernando earthquake (M_W 6.7). As shown by *Mori et al.* [1995] aftershocks of the San Fernando and Northridge events define a pair of conjugate planes reflecting regional northeast-southwest compression. Although the Northridge aftershocks grossly define the position of the southwest dipping rupture surface, they exhibit many complexities. In particular, they extend to shallower depths and further to the northwest than the slip plane inferred from seismic and geodetic studies of the main shock [e.g., *Wald et al.*, 1996]. Focal mechanism analyses of the Northridge aftershocks have shown a variety of different mechanisms, including both thrust and strike-slip faulting and a small number of normal faults [*Hauksson et al.*, 1995].

[4] The smaller magnitude events that dominate the Northridge sequence are recorded by the short-period stations of the Southern California Seismic Network (SCSN), operated jointly by the U.S. Geological Survey and the California Institute of Technology. These seismograms are examined by network operators who pick arrival times and measure *P* polarities used for routine locations and focal mechanisms but generally are not analyzed further. The data are, however, archived and made available to the research community through the Southern California Earthquake Center (SCEC) Data Center. Here we reexamine the Northridge aftershock sequence by applying waveform cross-correlation and other methods to short-period SCSN seismograms from 1981 to 1997, including data from about 15,000 events.

[5] Waveform cross-correlation techniques are useful both in characterizing the degree of event similarity [e.g., *Pechmann and Kanamori*, 1982; *Pechmann and Thorbjarnrdottir*, 1990; *Mezcua and Rueda*, 1994; *Menke*, 1999] and in facilitating more accurate relative locations within similar event clusters by providing more precise timing of *P* and *S* arrivals [e.g., *Nakamura*, 1978; *Poupinet et al.*, 1984; *Ito*, 1985; *Fremont and Malone*, 1987; *Xie et al.*, 1991; *Deichmann and Garcia-Fernandez*, 1992; *Aster and Scott*, 1993; *Got et al.*, 1994; *Dodge et al.*, 1995; *Haase et al.*, 1995; *Nadeau et al.*, 1995; *Gillard et al.*, 1996; *Phillips et al.*, 1997]. Our time domain analysis method (described by *Shearer* [1997, 1998], *Astiz and Shearer* [2000], and *Astiz et al.* [2000]) uses a natural neighbor approach to reduce the number of cross-correlations that must be computed. We find that about 10 to 30% of the Northridge aftershocks belong to similar event clusters, results comparable to other aftershock sequences in southern California but a lower percentage than recent studies of ongoing seismicity along active strands of the San Andreas and Hayward faults in central and Northern California [e.g., *Nadeau et al.*, 1995; *Rubin et al.*, 1999; *Waldhauser et al.*, 1999; *Waldhauser and Ellsworth*, 2000; *Rubin and Gillard*, 2000].

[6] The Northridge similar event clusters are amenable to more detailed analysis than is generally possible for individual earthquakes in southern California. Using differential times obtained from waveform cross-correlation, we relocate events within each cluster with a relative location accuracy of 50 m or better. These relocations often show planar features suggestive of faults at depth. By combining *P* polarity information from different events within each cluster we can obtain a consensus focal mechanism solution that is more reliable than the individual event focal mechanisms [e.g., *Shearer*, 1998]. A comparison of polarity measurement differences within similar event clusters provides constraints on the error rate in the individual polarity measurements and more reliable error estimates for individual event mechanisms. For some clusters, we are able to resolve the primary versus auxiliary fault plane ambiguity by comparing the computed focal mechanisms with the orientation of the plane that best fits the event locations. Our results show that the Northridge aftershocks define a very complex faulting regime, with thrust, oblique and strike-slip faulting occurring on faults of varying orientations.

2. Data and Processing

[7] We obtain waveforms from the SCSN as archived at the Southern California Earthquake Center (SCEC) Data

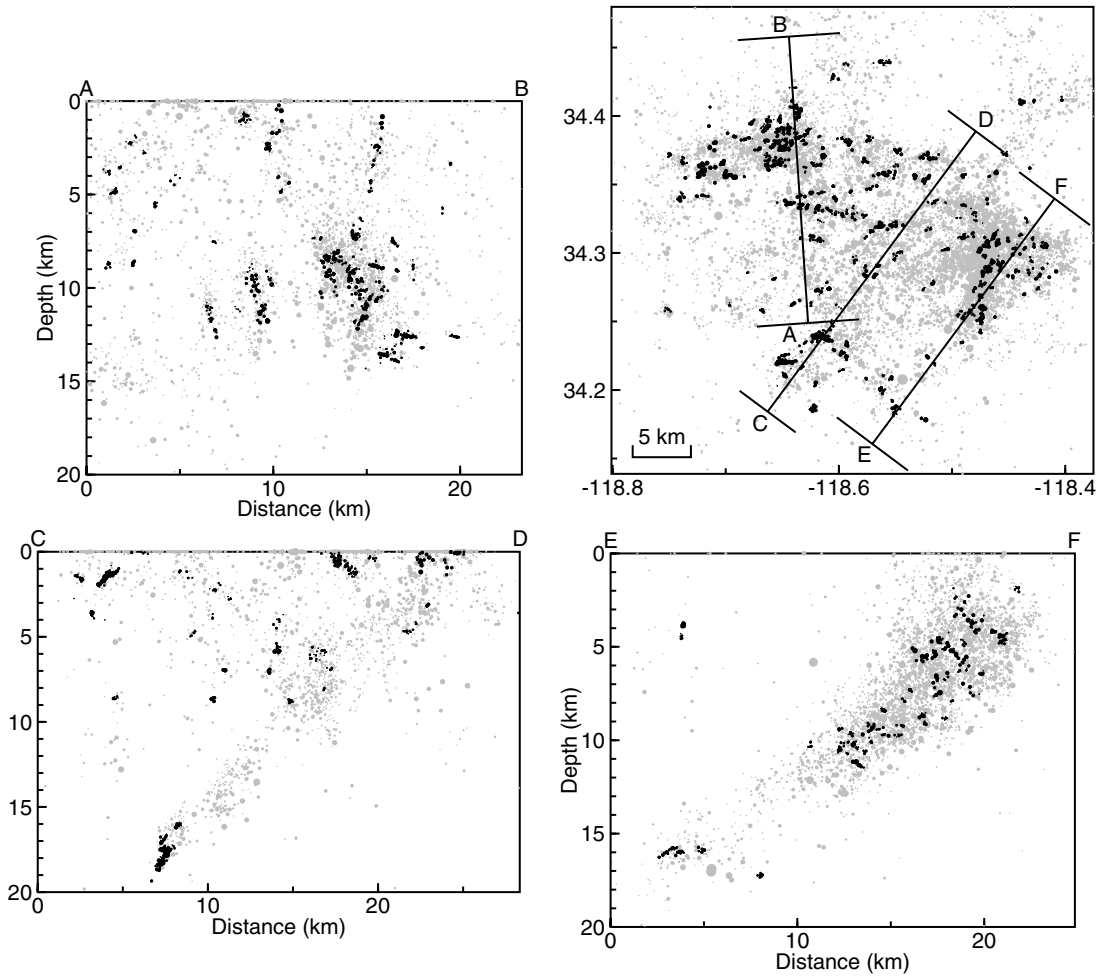

Figure 4. A map view and three cross-sections showing similar event clusters (black) with respect to the overall seismicity in the Northridge region. Symbol sizes scale with event magnitude.

Center for events from 1981 to 1997 with catalog locations within a box from 34.15 to 34.45°N, −118.75 to −118.25°E, resulting in a total of 15,029 events, of which 867 occurred prior to the Northridge main shock. To avoid ambiguities associated with the *Pg*/*Pn* crossover distance, we examine only the 148 stations located within 100 km of the center of the source region; however, most of the events are less than *M*2.5 and have archived waveforms from only 10 to 50 of these stations. Prior to the waveform cross-correlation, we resample the seismograms to a uniform 100 Hz sample rate and apply a 10-Hz low-pass filter. To speed the calculation, we restrict the waveform cross-correlation for each event to 100 neighboring events rather than the complete data set, using the Delaunay tesselation approach described by *Astiz and Shearer* [2000]. We compute the cross-correlation functions separately for the *P* and *S* waves using a 1.5 s window around *P* and a 3 s window around *S* and applying time shifts of up to ±1.5 s. Information is saved only for those event pairs with an average waveform correlation coefficient of 0.45 or greater and with at least 10 individual differential times with correlation coefficients of 0.6 or greater. Figure 3 plots examples of the waveform fit obtained for several different values of the correlation coefficient. Generally, reliable differential times are only obtained for correlations greater than 0.6.

[8] Differential time information can be incorporated into relocation algorithms in a number of different ways, from computing relative locations of separate event clusters [e.g., *Got et al.*, 1994] to combining differential times with absolute *P* and *S* picks, either by adjusting the pick times [*Shearer*, 1997] or applying the double-difference location method [*Waldhauser et al.*, 1999]. Experiments with relocating events within the 1998 Oak Ridge swarm, a compact cluster of ∼50 events about 20 km west of the Northridge aftershock zone, showed that the best locations were obtained using a relative location method applied to the differential times alone [*Shearer*, 1998]; we thus decided to adopt this approach for the Northridge aftershocks. This method reduces the problem to relocating events among

Table 1. Number of Clusters and Similar Events[a]

$\bar{r}_{min}$	nclust	nclust5	nev	nev5
0.70	513	33	1390	286
0.65	954	90	2912	904
0.60	1261	218	4831	2321
0.55	1211	272	7410	5133

[a]Where nclust = total number of similar event clusters, nclust5 = number of similar event, clusters with at least 5 events, nev = total number of events that are similar to at least one other event, and nev5 = number of events belonging to a similar event cluster with 5 or more events.

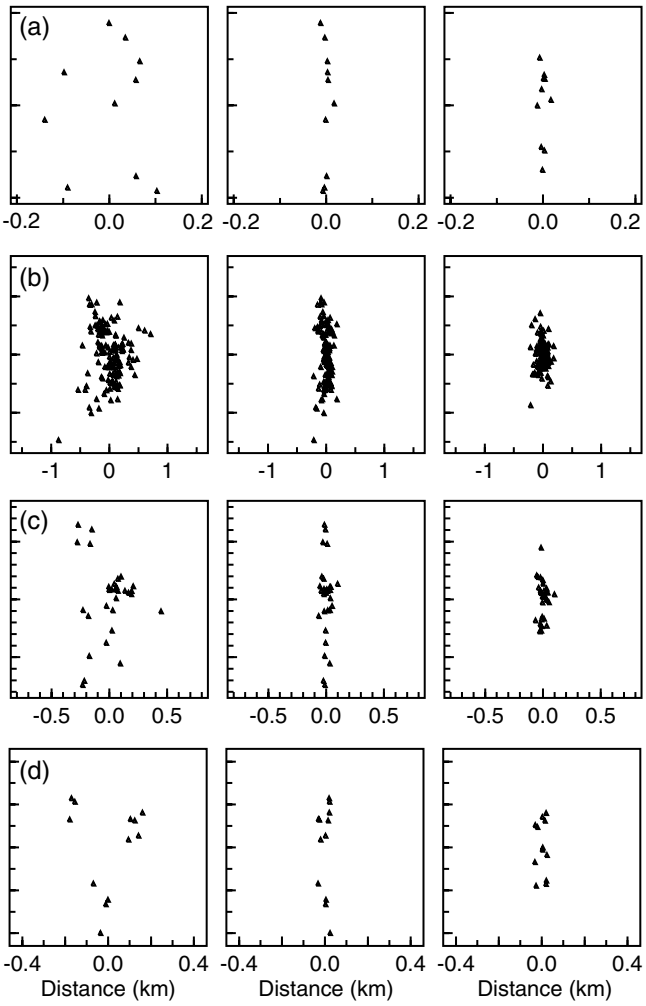

Figure 5. Seismicity in 4 similar event clusters plotted in a rotated coordinate system defined by principal component analysis (see text). Each of these clusters is roughly planar. The first column shows a "face-on" view of the cluster with events projected onto a plane perpendicular to the U_3 eigenvector; this plane is the best fitting plane to the cluster. The next two columns show projections defined by the U_2 and U_1 eigenvectors and provide "edge-on" views of the seismicity planes. The planarity of a cluster may be characterized by the ratio between the middle eigenvalue to the smallest eigenvalue (λ_2/λ_3). These clusters have λ_2/λ_3 values of (a) 149, (b) 8, (c) 33, and (d) 55.

each of a number of different similar event clusters; each cluster must be reasonably compact so that errors due to three-dimensional velocity structure outside the source region are nearly identical for all events within the cluster.

[9] The number and size of the similar event clusters will vary depending upon the criteria that are adopted to determine "similarity." We measure the degree of similarity between two events as the average of the individual P and S correlation coefficients for all stations recording both events. For events i and j, we term this average $\bar{r}_{ij}$ and require that $\bar{r}_{ij} \geq \bar{r}_{\min}$ for an event pair to be considered similar. Results listing the number of events obtained for various degrees of event similarity are summarized in Table 1. For $\bar{r}_{\min}$ values of 0.55, 0.60, 0.65 and 0.70 the number of events that are similar to at least one other event are 7410, 4831, 2912, and 1390, respectively (out of 15,030 total events). We define an event cluster as all of the events for which there is at least one connection path with $\bar{r}_{ij} \geq \bar{r}_{\min}$. Note that we do not require that all event pairs within the cluster exhibit this degree of similarity. Clusters with five or more events are the most useful because seismicity patterns (e.g., lines, planes, etc.) can often be discerned and errors are more easily estimated by checking the consistency of the differential times. A smaller fraction of the total events are found in groups of this size (see Table 1). The results shown in this paper are based on $\bar{r}_{\min} = 0.60$, a value which represents a compromise between the high precision that is possible for very similar event pairs and the larger number of events that can be assigned to clusters for less similar event pairs. Experiments with higher values of $\bar{r}_{\min}$ suggest that comparable results to those presented here could be obtained, albeit for a smaller number of events.

[10] Next, we relocate the events within each of the 218 clusters containing 5 or more events using the differential times obtained from cross-correlation and the grid-search, L1-norm method described by *Shearer* [1998]. Starting locations are obtained from the relocated SCSN catalog of *Richards-Dinger and Shearer* [2000]. We use a smooth version of the *Hadley and Kanamori* [1977] velocity model for southern California. Median estimated relative location standard errors for events within each cluster are 22 m in horizontal position and 32 m in-depth. Results of these relocations are shown in Figure 4 in map view and three different vertical cross-sections. Note that usually, but not always, the orientation of the events within individual clusters agrees with the gross trend of the seismicity in the vicinity of the cluster. For example, the deep clusters shown in cross-sections CD and EF are aligned parallel to the southwest dipping trend of the main shock fault plane. Similarly, many of the clusters shown in cross-section AB, in the northwest corner of the Northridge aftershock distribution, are vertically aligned, agreeing with the vertical trends shown in the background seismicity in this region. However, cross-section EF shows a seismicity cluster (near 11.5 km depth) that appears to be oriented perpendicular to the main shock fault plane. Similarly, there are several near-horizontal clusters in cross-section AB which cut across the general vertical trend of other seismicity in this region. We will discuss these features at greater length later in the paper.

3. Fitting Planes to the Seismicity Clusters

[11] Although the orientation of the seismicity within similar event clusters can be determined by making suitable cross-sections, it is desirable to have a more automated method for large-scale data processing. Here we use the method of principal component analysis [e.g., *Kirschvink*, 1980]; this approach was previously applied to earthquake locations by *Michelini and Bolt* [1986]. Define the 3×3 matrix $\mathbf{V}$ as the covariance of the x_1, x_2 and x_3 coordinates of the event locations with respect to their means:

$$V_{ij} = 1/m \sum_{k=1}^{m} \left(x_i^k - \bar{x}_i\right)\left(x_j^k - \bar{x}_j\right) \qquad i,j = 1,2,3$$

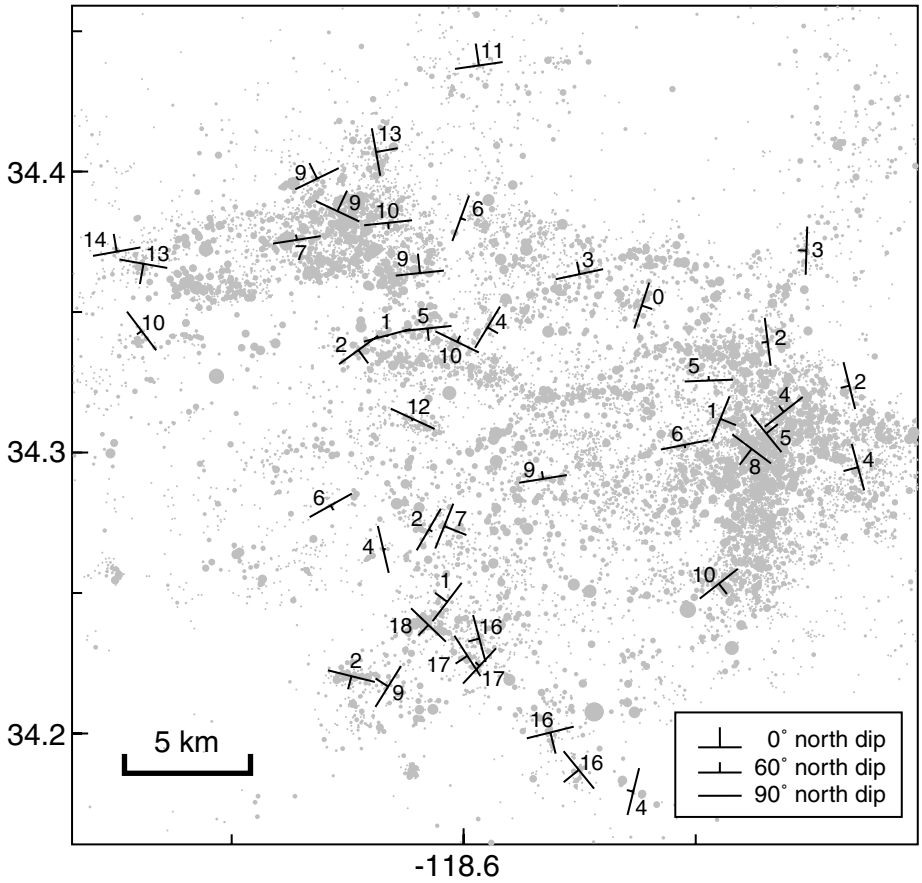

Figure 6. Orientations of similar event cluster seismicity planes as determined using principal component analysis. Strike is shown with the longer line; the dip direction and magnitude are indicated by the direction and length of the shorter line. The numbers give the depth in kilometers of the center of each cluster.

where m is the number of events and $\bar{\mathbf{x}}$ is the mean location. The eigenvalues of $\mathbf{V}$ (λ_i where $\lambda_1 \geq \lambda_2 \geq \lambda_3$) and the corresponding eigenvectors U_1, U_2 and U_3 define the principal axes of rotational inertia for these points. Eigenvector U_1, corresponding to the largest eigenvalue, gives the axis of minimum rotational inertia, and defines the longest axis of an ellipsoid fit to the original points, while U_3, corresponding to the smallest eigenvalue, defines the shortest axis of the ellipsoid. The shape of the seismicity cluster can be characterized by the relative sizes of the eigenvalues. A nearly spherical distribution of events will have $\lambda_1 \approx \lambda_2 \approx \lambda_3$. Points aligned linearly along a line will have $\lambda_1 \gg \lambda_2, \lambda_3$ with U_1 defining the direction of the line. Points flattened into a plane will have $\lambda_3 \ll \lambda_1, \lambda_2$ with U_3 orthogonal to the plane. Moreover, it can be shown that U_1 and U_3 correspond to the least squares solutions (perpendicular distance) for the best fitting line and plane, respectively.

[12] Using this approach, we compute eigenvalues for the covariance matrix of the locations for all similar event clusters with 5 or more events. We consider the cluster to have a well-defined seismicity plane if $\lambda_2/\lambda_3 \geq 8$ and the standard error of the plane orientation, estimated using a bootstrap resampling procedure, does not exceed 20°. It is natural to assume that these seismicity planes define the position and orientation of subsurface faults and we will sometimes use the term ''fault'' to describe these patterns. However, it should be kept in mind that this interpretation may not always be correct; there could be a structural feature, such as a weak zone or fluid conduit, that facilitates earthquake occurrence without actually defining a fault plane on which each event slips.

[13] Locations plotted in the principal axes coordinate system are shown for some of the larger clusters in Figure 5. These plots show one face-on view and two edge-on views for each seismicity plane. Figure 6 shows the orientation and dip of 45 aftershock seismicity planes measured using this method. Most planes are steeply dipping; the average dip angle is 58°. Fault strikes and dip directions vary widely, especially for events near the eastern side of the aftershock zone. Fault strikes in the northwest cluster are more consistent, generally striking approximately east-west. Two large aftershocks (M_W 4.5) in this region occurred on 26/27 April 1997, at about 34.38°N, 118.66°W. Clusters in this area are steeply dipping to the south-southwest, in agreement with rupture planes obtained for these events by *Venkataraman et al.* [2000]. At depths near the main shock rupture plane, several clusters agree roughly with the main shock strike and dip. Other nearby clusters, however, are at markedly different angles. The overall picture is one of great complexity with sharp changes in fault orientation seen over relatively short distances.

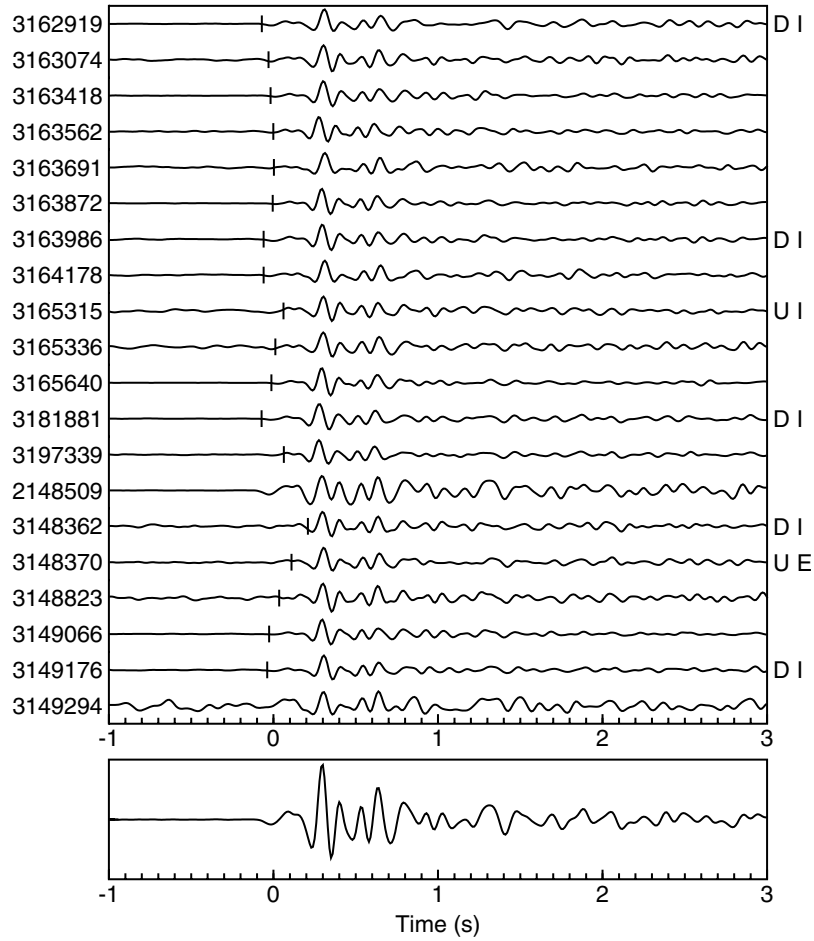

Figure 7. P wave seismograms recorded at station WSP for 20 events within a Northridge similar event cluster. The SCSN operator *P* picks are indicated. Polarity measurements, when available, are shown to the right (U = up, D = down, I = impulsive, E = emergent). SCSN event cusp ID numbers are listed to the left. The bottom waveform is a stack of the 20 individual seismograms and clearly shows the downward first motion of these traces. Note the scatter in the *P* picks and the occasional upward polarity pick.

[14] Although the aftershock pattern grossly follows the main shock rupture plane in many regions, the fine-scale details of the seismicity suggest that these events do not fall on a single rupture plane, but rather occur within a ''damage zone'' of several kilometers width. This is suggested by the differing orientations of the similar event clusters within the zone and the fact that the estimated errors in the aftershock locations are much less than the width of the zone. An aftershock zone of measurably finite width also occurred along the 1992 Landers earthquake rupture surface [*Liu et al.*, 1999].

4. Composite Focal Mechanism Analysis

[15] Focal mechanisms for small earthquakes in southern California are routinely computed using *P* first motions measured by the SCSN operators. However, poor signal-to-noise can often introduce uncertainties into polarity observations and errors into the resulting focal mechanisms. The existence of similar event clusters makes it possible to compute focal mechanisms more accurately than can be done for individual events. This is illustrated in Figure 7 which plots waveforms for events within a single similar event cluster recorded at station WSP. The SCSN phase picks and *P* first motion measurements are also marked. Plotting the events in this way shows how variable signal-to-noise levels in the records can introduce inconsistencies into the measurements. The scatter in the travel time picks can be greatly reduced by using waveform cross-correlation to align the phases, leading to much more precise relative event locations. Furthermore, the similarity in the observed waveforms suggests that the focal mechanisms for the events within each event cluster are nearly identical and that the first motion measurements at a particular station should not vary among events.

[16] The consistency of the *P* first-motion measurements for a given similar event cluster can be improved by stacking the waveforms and picking the polarity by hand, or, more easily, by simply using the consensus of the previously measured polarities at each station (both techniques are discussed at greater length by *Shearer* [1998]). The resulting set of ''composite'' first motion measurements for the cluster is typically larger (more stations) and more

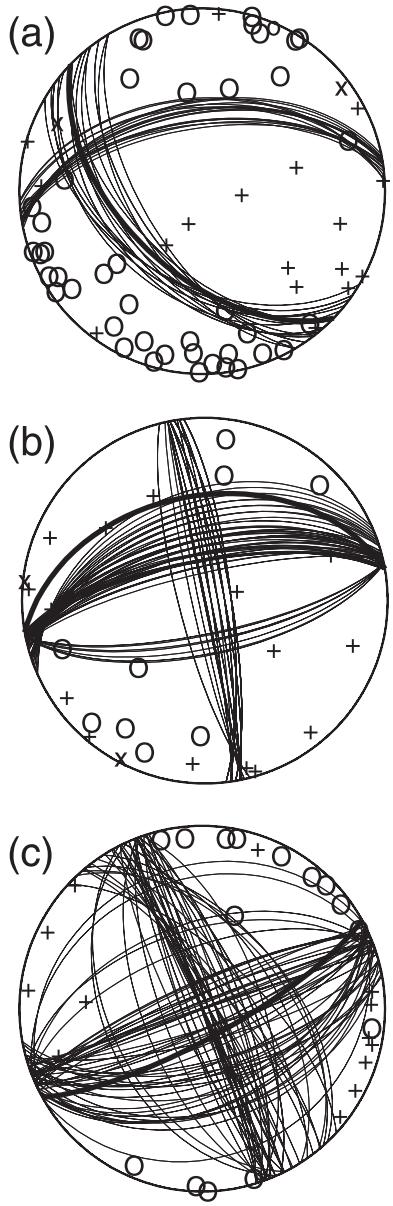

Figure 8. Lower hemisphere focal spheres for three different Northridge similar event clusters. Consensus polarity measurements are shown with "+" for upward first motion and "○" for downward first motion. For most stations the majority of the measurements are from arrivals labeled as "impulsive." Cases where the "emergent" arrivals are more numerous are indicated with "×" and a smaller "○," respectively. The thin lines indicate the acceptable focal mechanisms returned by a grid search technique. The thick lines show the orientation of the seismicity plane for each cluster as determined by principal component analysis.

accurate than the data available for any individual event within the cluster. Here we apply the consensus polarity approach to computing focal mechanisms for the Northridge aftershock similar event clusters. To assign a polarity to a given station, we require 3 or more measurements with at least 2/3 of the measurements having the same polarity. We compute take-off angles and azimuths based on the same smoothed version of the *Hadley and Kanamori* [1977] velocity model that was used to locate the events. Focal mechanisms are then computed using a grid-search method similar to FPFIT [*Reasenberg and Oppenheimer*, 1985], but which returns more detailed error estimates for the mechanisms [*Hardebeck and Shearer*, 2002].

[17] Examples of this method applied to three different clusters are shown in Figure 8. The thin lines show the different acceptable focal mechanisms returned by the grid search method. In the top example (Figure 8a), there is some scatter in the solutions but the mechanism is reasonably well constrained by the polarity data. It is mainly thrust with a small strike-slip component. The thick line shows the best fitting seismicity plane for this cluster as determined by the covariance matrix method (see above). In this case, there is good agreement between this southward dipping plane and one of the two possible fault planes defined by the focal mechanism. We are thus in the fortunate position of not only having a check on the two approaches but being able to resolve the primary versus auxiliary plane ambiguity that is inherent in focal mechanism analyses. For this example, we may infer that the fault plane dips at $\sim 60^\circ$ to the southwest. In the second example (Figure 8b), the polarity data resolve the strike of both nodal planes but there is some ambiguity regarding the dip of the east-west trending plane. The seismicity plane, shown as the thick line, can be used to resolve this ambiguity. In the third example (Figure 8c), the polarity data permit considerable scatter in the dip of both nodal planes. The seismicity plane can help resolve the true dip of the east-west trending plane, but there remains some uncertainty in the dip of the second nodal plane. In these last two examples, the orientation of the seismicity plane does not really provide an independent check on the validity of the mechanism, but can be used to compute a better constrained mechanism than could be obtained from the polarity data alone.

[18] In some cases, there are discrepancies between the computed focal mechanisms and the seismicity planes. We suspect that in most cases these disagreements reflect inaccuracies in the focal mechanisms, particularly for shallow events where the takeoff angles are poorly determined [e.g., *Hardebeck and Shearer*, 2002]. It is also possible that the seismicity plane does not define the slip plane for these events, as may be the case [see *Shearer*, 1998] for the Oak Ridge cluster to the west of the Northridge aftershock zone. This is an issue that warrants further study; clearly, however, contradictory results between the methods cast some doubt on the reliability of the focal mechanisms in these cases. Thus, in this paper we choose to disregard the composite focal mechanisms that do not agree with the seismicity planes and focus our analysis on those mechanisms for which one of the acceptable fault planes is within 30° of the seismicity plane. Figure 9 plots these results for 21 composite focal mechanisms, with the true fault planes marked in black as inferred from the seismicity planes. A comparison of Figure 6 and Figure 9 shows that we were able to compute seismicity-plane-consistent focal mechanisms for about 50% of the clusters with clear seismicity planes.

[19] The composite focal mechanisms show southward dipping thrust faults at 15 to 20 km depth, roughly parallel to the main shock rupture plane. However, the two

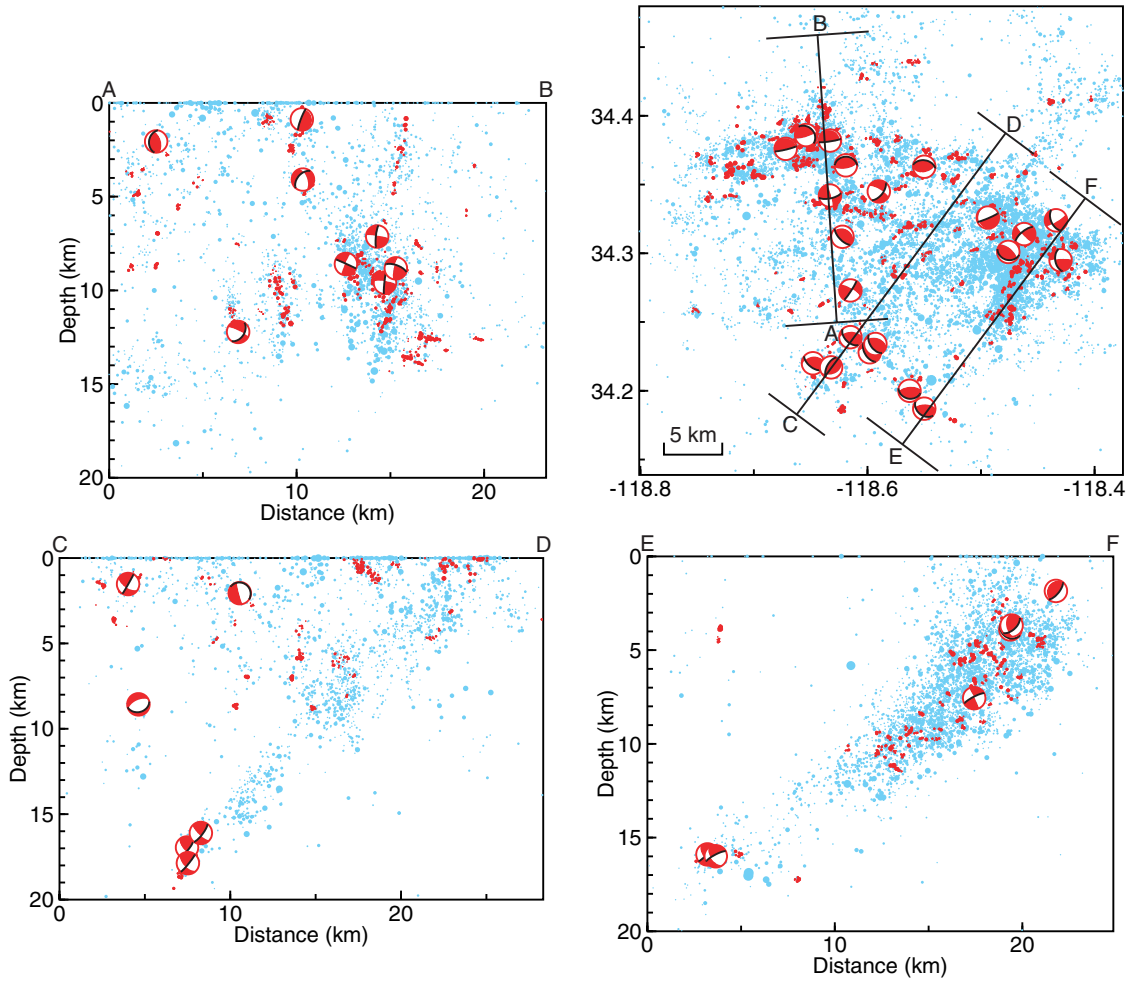

Figure 9. Composite focal mechanisms for Northridge similar event clusters as shown in map view and three different cross-sections. Lower hemisphere focal spheres are plotted in the map view; far-side focal spheres are plotted in the cross-sections. The true fault planes, as determined by the seismicity plane for each cluster, are indicated by the black lines on the focal spheres. Focal spheres and other similar event seismicity are shown in red, background seismicity is shown in blue.

mechanisms near 16 km depth in profile EF (Figure 9) have rupture planes with dips of 26° to 36°, significantly shallower than the 54° to 62° dip of the three deep mechanisms in profile CD to the northwest. This is consistent with previous results that have shown that the aftershock zone steepens from east to west [*Hauksson et al.*, 1995]. The mechanisms at shallower depths are less consistent in both strike and dip and indicate a more complicated system of faults. For example, the five northeast mechanisms in Figure 9 contain strike-slip, oblique, and reverse faults at both shallow and steep dip angles. Four composite mechanisms in the northwest part of Figure 9 at depths of 7 to 10 km are particularly interesting because their focal mechanisms appear nearly identical, but their slip planes, as indicated by the fit to the seismicity, are very different. Two of the clusters occurred on steep southward-dipping planes, in contrast to the shallow northward-dipping planes of the other two clusters. Apparently there are two main types of faulting in this region: near-vertical, east-west trending faults and near-horizontal faults that are approximately orthogonal to each other. This can also be seen directly in the AB profile in Figure 4. This example suggests that it may be dangerous to assume that nearby events with similar focal mechanisms occurred on faults with similar orientations; both nodal planes may be active.

[20] *Hadley and Kanamori* [1978] and *Webb and Kanamori* [1985] observed deep events with shallow-dipping nodal planes that they suggested may be evidence for a regional subhorizontal decollement. Our analysis resolves a number of shallow-dipping fault planes in the Northridge events that extend to depths of up to 16 km. However, as noted by *Hauksson et al.* [1995], the Northridge sequence includes many events at greater depths so these shallow fault planes do not define the base of the seismogenic zone. In addition, the shallow-dipping planes occur at a variety of depths; there does not seem to be a single near-horizontal fault beneath the whole region. In general, the composite focal mechanisms are quite varied, even on short spatial scales, with both strike-slip and reverse faulting, suggesting a complicated faulting regime. The composite results are, however, limited to a small number of similar event clusters.

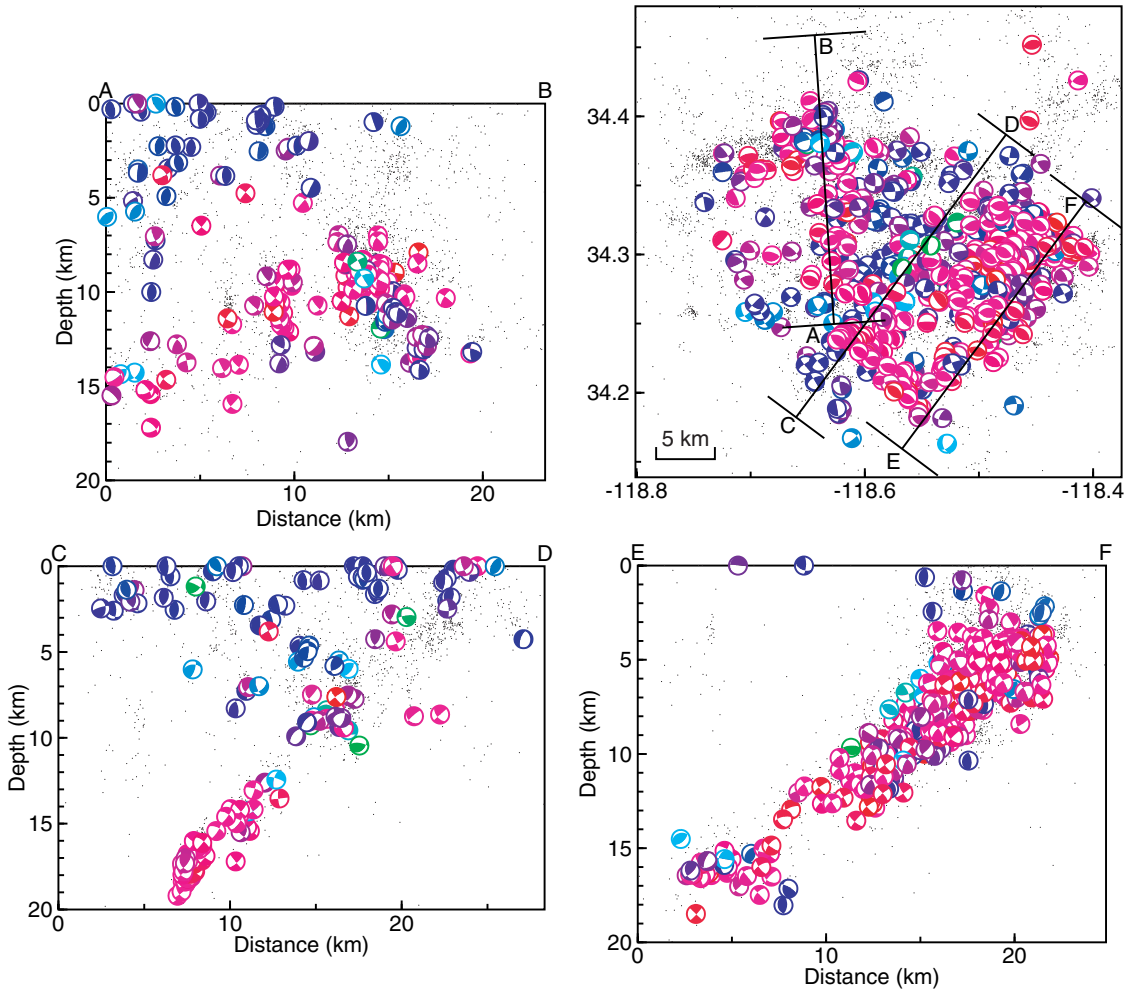

Figure 10. Single event focal mechanisms for 782 Northridge earthquakes in map view and three cross-sections. The focal mechanism color represents the style of slip, and is gradational from red for pure thrust, to blue for pure strike-slip, to green for pure normal faulting. Only mechanisms which are stable with respect to errors in source location, seismic velocity model and polarity observations are shown, the remaining seismicity is shown in black.

To obtain more complete coverage, we need to examine individual event focal mechanisms.

5. Single Event Focal Mechanism Analysis

[21] Single event focal mechanisms for the Northridge sequence are determined using the method of *Hardebeck and Shearer* [2002]. This method is different from the well-known FPFIT algorithm [*Reasenberg and Oppenheimer*, 1985] in that it identifies a set of acceptable solutions for each event, given the uncertainty in source location, seismic velocity model and polarity observations. If the set of acceptable mechanisms is tightly clustered around the preferred mechanism, the solution is stable with respect to errors. Only if the RMS angular difference between the acceptable mechanisms and the preferred mechanism is less than 35° is a solution considered to be adequately stable.

[22] The similar event clusters can be used to estimate the actual rate of polarity errors in the Northridge data set. Assuming that the events in each cluster have the same mechanism, the observed polarity at a given station should be the same for each event in a cluster. For all of the similar event clusters, we find that ~10% of the impulsive P polarities are inconsistent. Therefore, mechanisms with up to ~10% misfit polarities are included in the set of acceptable mechanisms.

[23] The 782 earthquakes for which stable single event focal mechanisms can be found are predominately thrust, but also include many strike-slip and a few normal faulting mechanisms (Figures 10 and 11.) Although all three styles of faulting occur throughout the Northridge region, the events occurring along the main shock fault plane are predominately thrust, while those in the hanging wall and footwall are predominately strike-slip. The mechanisms are often locally coherent. Spatially close events tend to exhibit similar focal mechanisms, especially along and above the Northridge main shock rupture (Figure 10, cross-sections CD and EF.)

[24] The events occurring along the rupture zone of the Northridge main shock are predominately thrust, with the south-dipping plane generally subparallel to the fault plane of the main shock. The T axes are near vertical (Figures 12c and 12f), while most of the P axes trend N to N60°E. The seismicity in the hanging wall, on the other hand, exhibits primarily strike-slip mechanisms, with the P axes oriented

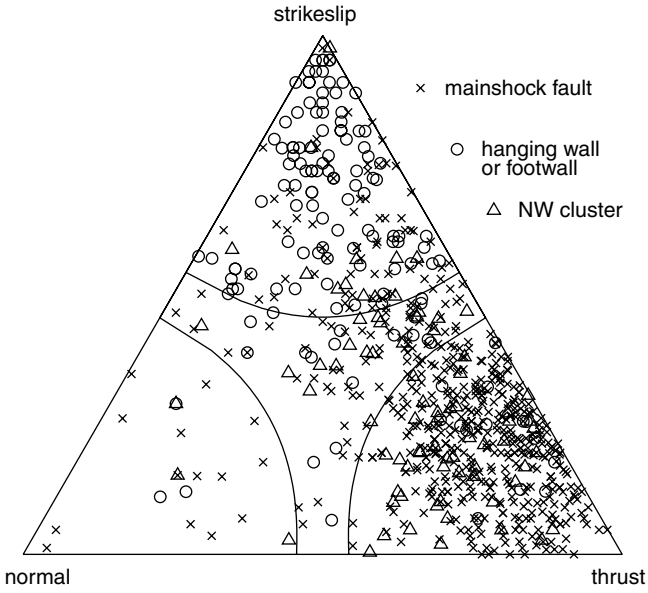

Figure 11. Triangle diagram indicating the proportions of strike-slip, normal, and thrust motion for each of the 782 Northridge earthquakes for which single-event first motion focal mechanisms were found. The position on the diagram is determined from the plunge of the P, T, and B axes, following *Frohlich* [2001]. The solid curves indicate a plunge of 50°. The events are divided into three sets: those occurring along the main Northridge rupture, those in the hanging wall or footwall, and those in the cluster to the northwest of the main shock.

N to N60°E (Figures 12b and 12e), similar to the P axes of the along-fault thrust events. Focal mechanisms were found for one group of footwall events, at ~10 km depth in cross-section CD, which are predominately slightly oblique strike-slip. These mechanisms are within the scatter of the strike-slip mechanisms observed in the hanging wall, although the average trends of the P and T axes are rotated ~15° clockwise (Figure 12d).

[25] The patterns of focal mechanisms are similar to those observed by *Hauksson et al.* [1995] and *Unruh et al.* [1997]. *Unruh et al.* [1997] proposed that the seismicity is accommodating NNE–SSW shortening, which is balanced by vertical thickening due to thrust faulting along the Northridge main shock fault plane and by WNW–ESE lengthening due to strike-slip and normal faulting in the hanging wall. This model is generally supported by the single event focal mechanisms found in this study. However, *Unruh et al.* [1997] assume that the footwall is not deforming, although there is clearly aftershock activity. The focal mechanisms suggest that in the footwall, as in the hanging wall, the NE–SW to NNE–SSW shortening is balanced by NW–SE to WNW–ESE extension accommodated by strike-slip faulting.

[26] It has been proposed that the stress field, and therefore the pattern of earthquake focal mechanisms, changed through time as a result of the Northridge main shock [*Zhoa et al.*, 1997]. *Zhoa et al.* [1997] observed a ~20° counterclockwise stress rotation at the time of the main shock, followed by a return to the original stress state over the next two years. Stable single event focal mechanisms could be found for only

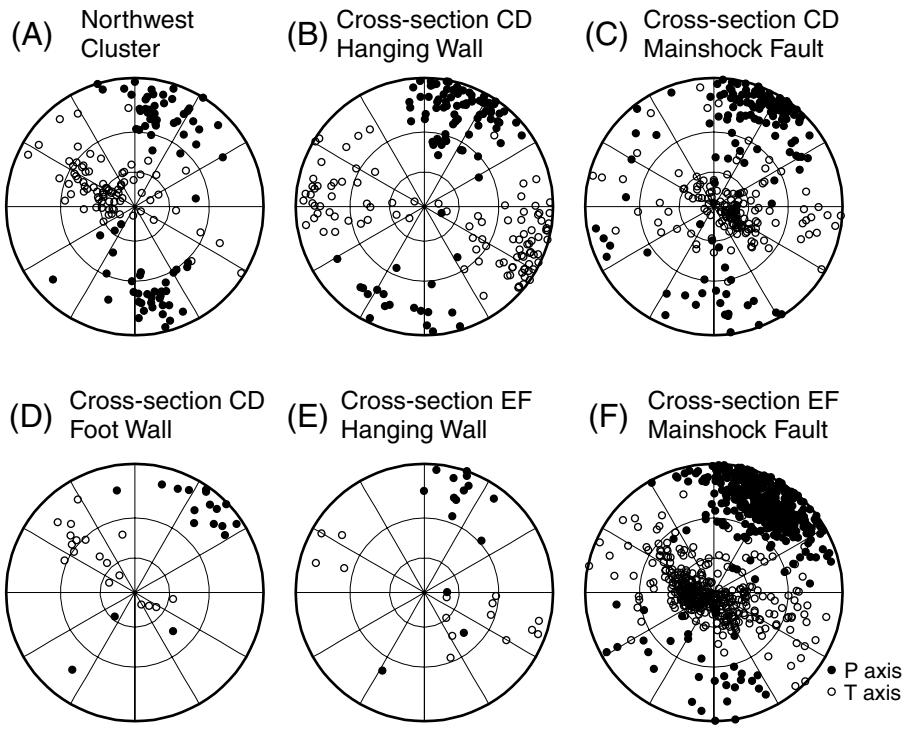

Figure 12. Lower hemisphere projections of the P axes (solid circles) and T axes (open circles) of the single event focal mechanisms for events (A) in the cluster to the northwest of the Northridge main shock, (B) in the hanging wall in cross-section CD (Figure 11), (C) in a 5-km-wide zone along the main shock rupture in cross-section CD, (D) in the footwall in cross-section CD, (E) in the hanging wall in cross-section EF, (F) in a 10-km-wide zone along the main shock rupture in cross-section EF.

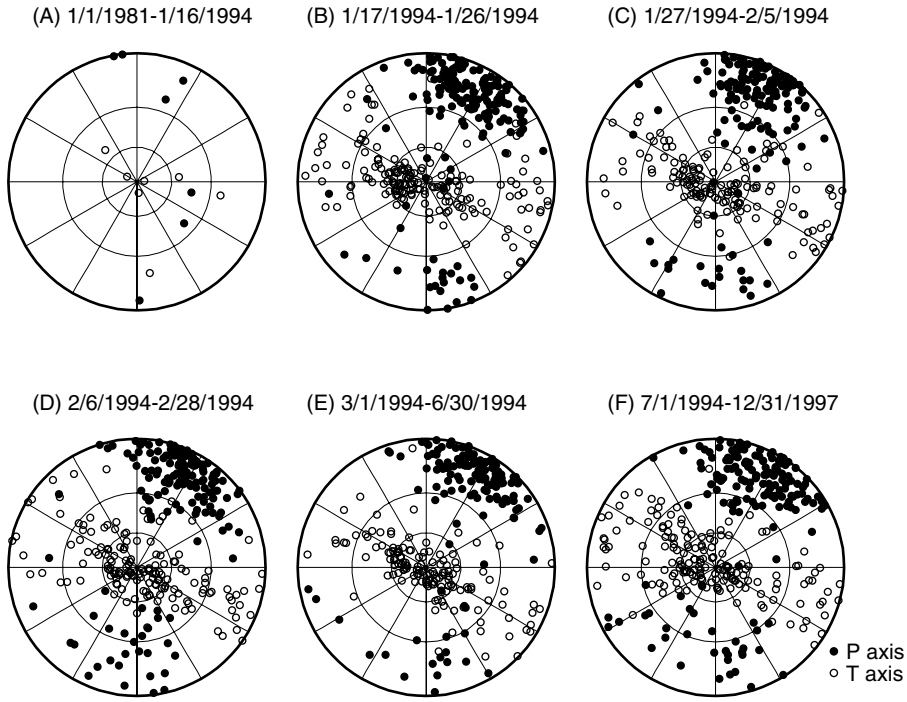

Figure 13. Lower hemisphere projections of the P axes (solid circles) and T axes (open circles) of all single event focal mechanisms for six time intervals.

seven premain shock events, so we cannot detect a coseismic change in the focal mechanisms. No postseismic rotation of the P axes or T axes is apparent (Figure 13).

6. Discussion

[27] This work is part of our ongoing effort to compute improved locations for southern California earthquakes using waveform cross-correlation and other techniques [*Shearer*, 1997, 1998; *Astiz and Shearer*, 2000; *Astiz et al.*, 2000; *Richards-Dinger and Shearer*, 2000]. Advances made in this study include (1) processing of far more events (~15,000) than the prior analyses, (2) separate relocation of different similar event clusters within a distributed region of seismicity, (3) application of principal component analysis to the relocated event clusters, (4) calculation of consensus *P* first-motion polarities and composite focal mechanisms for similar event clusters, and (5) association of seismicity planes with focal mechanism planes to resolve fault plane ambiguities.

[28] Results of this study have also been useful in designing a new method for computing individual focal mechanisms from *P* polarity data [*Hardebeck and Shearer*, 2002] by using similar event clusters to estimate the average rate of *P* polarity measurement errors in the Northridge data set. Individual event focal mechanisms determined for 782 Northridge events show a range of different mechanisms, with thrust faulting occurring predominantly along the main shock fault plane and strike-slip faulting occurring in the hanging wall and footwall.

[29] It should be emphasized that the improvements in event location accuracy shown here are for the relative locations of events within similar event clusters; the absolute location of each cluster is determined by its starting location, in this case the catalog of *Richards-Dinger and Shearer* [2000]. A minority of Northridge aftershocks belong to similar event clusters (10 to 30%, depending upon the selection criteria), in rough agreement with the relatively low degree of similarity observed in other southern California aftershock sequences, such as Whittier Narrows, Upland and Oceanside [*Shearer*, 1997; *Astiz and Shearer*, 2000; *Astiz et al.*, 2000]. This contrasts with the high similarity rates observed along active portions of the San Andreas Fault in northern California, such as the 63% rate noted by *Nadeau et al.* [1995] near Parkfield and the 75% rate seen by *Rubin et al.* [1999] near San Jaun Bautista. It is not yet clear if low event similarity rates in southern California are specific to aftershock sequences or if they represent a more general difference in the style of faulting between northern and southern California.

[30] Our results are in reasonable agreement with previous aftershock analyses, both in the locations of the events and in the type of faulting. Thus, we do not include here a detailed comparison between the aftershock pattern and the local geology and tectonics, as was done by *Hauksson et al.* [1995]. Our results, however, do provide greater resolution in many areas and address several issues in more detail than prior studies. This includes direct discrimination between the primary and auxiliary fault planes for 21 similar event composite focal mechanisms, revealing both shallow- and steeply dipping reverse faulting in several areas. Results from an analysis of individual event focal mechanisms indicate mainly thrust faulting near the main shock rupture plane and mostly strike-slip faulting in the hanging wall. We observe no rotation of the P or T axes during the postseismic period. Finally, the aftershock

zone is at least 2 to 3 km wide, even in its narrowest parts. The aftershocks do not define a single fault surface; rather they appear to illuminate complicated and often overlapping patterns of faulting.

[31] **Acknowledgments.** We thank the personnel of the USGS/Caltech Southern California Seismic Network who pick and archive the seismograms and the Southern California Earthquake Center (SCEC) for distributing the data; we especially thank Katrin Hafner, who facilitated access to the database. Cliff Frohlich, Yosio Nakamura and an anonymous reviewer provided useful comments. Funding for this research was provided by NEHRP/USGS grants 1434-HQ-97-GR-03162 and 00HQGR0057. This research was also supported by SCEC, which is funded by NSF Cooperative Agreement EAR-8920136 and USGS Cooperative Agreements 14-08-0001-A0899 and 1434-HQ-97AG01718. The SCEC contribution number for this paper is 653.

References

Aster, R. C., and J. Scott, Comprehensive characterization of waveform similarity in microearthquake data sets, *Bull. Seismol. Soc. Am.*, *83*, 1307–1314, 1993.

Astiz, L., and P. M. Shearer, Earthquake locations in the inner Continental Borderland, offshore southern California, *Bull. Seismol. Soc. Am.*, *90*, 425–449, 2000.

Astiz, L., P. M. Shearer, and D. C. Agnew, Precise relocations and stress change calculations for the Upland earthquake sequence in southern California, *J. Geophys. Res.*, *105*, 2937–2953, 2000.

Deichmann, N., and M. Garcia-Fernandez, Rupture geometry from high-precision relative hypocentre locations of microearthquake ruptures, *Geophys. J. Int.*, *110*, 501–517, 1992.

Dodge, D. A., G. C. Beroza, and W. L. Ellsworth, Foreshock sequence of the 1992 Landers, California, earthquake and its implications for earthquake nucleation, *J. Geophys. Res.*, *100*, 9865–9880, 1995.

Fremont, M.-J., and S. D. Malone, High precision relative locations of earthquakes at Mount St. Helens, Washington, *J. Geophys. Res.*, *92*, 10,223–10,236, 1987.

Frohlich, C., Display and quantitative assessment of distributions of earthquake focal mechanisms, *Geophys. J. Int.*, *144*, 300–308, 2001.

Gillard, D., A. M. Rubin, and P. Okubom, Highly concentrated seismicity caused by deformation of Kilauea's deep magma system, *Nature*, *384*, 343–346, 1996.

Got, J.-L., J. Fréchet, and F. W. Klein, Deep fault plane geometry inferred from multiplet relative relocation beneath the south flank of Kilauea, *J. Geophys. Res.*, *99*, 15,375–15,386, 1994.

Haase, J. S., P. M. Shearer, and R. C. Aster, Constraints of temporal variations in velocity near Anza, California, from analysis of similar event pairs, *Bull. Seismol. Soc. Am.*, *85*, 194–206, 1995.

Hadley, D. M., and H. Kanamori, Seismic structure of the Transverse Ranges, California, *Geol. Soc. Am. Bull.*, *88*, 1461–1478, 1977.

Hadley, D. M., and H. Kanamori, Recent seismicity in the San Fernando region and tectonics in the west-central Transverse Ranges, California, *Bull. Seismol. Soc. Am.*, *68*, 1449–1457, 1978.

Hardebeck, J. L, and P. M. Shearer, A new method for determining first-motion focal mechanisms, *Bull. Seismol. Soc. Am.*, in press, 2002.

Hauksson, E., Earthquake, faulting, and stress in the Los Angeles Basin, *J. Geophys. Res.*, *95*, 15,365–15,394, 1990.

Hauksson, E., Crustal structure and seismicity distribution adjacent to the Pacific and North American plate boundary in southern California, *J. Geophys. Res.*, *105*, 13,875–13,903, 2000.

Hauksson, E., and J. S. Haase, Three-dimensional V_P and V_P/V_S velocity models of the Los Angeles basin and central Transverse Ranges, California, *J. Geophys. Res.*, *102*, 5423–5433, 1997.

Hauksson, E., L. M. Jones, and K. Hutton, The 1994 Northridge earthquake sequence in California: Seismological and tectonic aspects, *J. Geophys. Res.*, *100*, 12,335–12,355, 1995.

Huftile, G. J., and R. S. Yeats, Deformation rates across the Placerita (Northridge M_W = 6.7 aftershock zone) and Hopper Canyon segments of the western Transverse Ranges deformation belt, *Bull. Seismol. Soc. Am.*, *86*, S3–S18, 1996.

Ito, A., High solution relative hypocenters of similar earthquakes by cross-spectral analysis method, *J. Phys. Earth*, *33*, 279–294, 1985.

Kirschvink, J. L., The least-squares line and plane and the analysis of palaeomagnetic data, *Geophys. J. R. Astron. Soc.*, *62*, 699–718, 1980.

Liu, J., K. E. Sieh, and E. Hauksson, Aftershocks and structural geology: Suggestions from the 1992 Landers earthquake sequence, *EOS Trans. AGU*, *80*(46), Fall Meet. Suppl., F650–F651, 1999.

Menke, W., Using waveform similarity to constrain earthquake locations, *Bull. Seismol. Soc. Am.*, *89*, 1143–1146, 1999.

Mezcua, J., and J. Rueda, Earthquake relative location based on waveform similarity, *Tectonophysics*, *233*, 253–263, 1994.

Michelini, A., and B. A. Bolt, Application of the principal parameter method to the 1983 Coalinga, California, aftershock sequence, *Bull. Seismol. Soc. Am.*, *76*, 409–420, 1986.

Mori, J., D. J. Wald, and R. L. Wesson, Overlapping fault planes of the 1971 San Fernando and 1994 Northridge, California, earthquakes, *Geophys. Res. Lett.*, *22*, 1033–1036, 1995.

Nadeau, R. M., W. Foxall, and T. V. McEvilly, Clustering and periodic recurrence of microearthquakes on the San Andreas Fault at Parkfield, California, *Science*, *267*, 503–507, 1995.

Nakamura, Y., A1 moonquakes: Source distribution and mechanism, *Proc. Lunar Planet. Sci. Conf., IXth*, 3589–3607, 1978.

Pechmann, J. C., and H. Kanamori, Waveform and spectra of preshocks and aftershocks of the 1979 Imperial Valley, California, earthquake: A test of the asperity model, *J. Geophys. Res.*, *87*, 10,579–10,597, 1982.

Pechmann, J. C., and B. S. Thorbjarnrdottir, Waveform analysis of two preshock-main shock-aftershock sequences in Utah, *Bull. Seismol. Soc. Am.*, *80*, 519–551, 1990.

Phillips, W. S., L. S. House, and M. C. Fehler, Detailed joint structure in a geothermal reservoir from studies of induced microearthquake studies, *J. Geophys. Res.*, *102*, 11,745–11,763, 1997.

Poupinet, G., W. L. Ellsworth, and J. Frechet, Monitoring velocity variations in the crust using earthquake doublets: An application to the Calaveras Fault, California, *J. Geophys. Res.*, *89*, 5719–5731, 1984.

Pujol, J., An integrated 3D velocity inversion—Joint hypocentral determination relocation analysis of events in the Northridge area, *Bull. Seismol. Soc. Am.*, *86*, S138–S155, 1996.

Reasenberg, P., and D. Oppenheimer, FPFIT, FPPLOT, and FPPAGE: FORTRAN computer programs for calculating and displaying earthquake fault-plane solutions, *U.S. Geol. Surv. Open File Rep. 85-739*, 109 pp., 1985.

Richards-Dinger, K. B., and P. M. Shearer, Earthquake locations in southern California obtained using source-specific station terms, *J. Geophys Res.*, *105*, 10,939–10,960, 2000.

Rubin, A. M., and D. Gillard, Aftershock asymmetry/rupture directivity among central San Andreas fault microearthquakes, *J. Geophys. Res.*, *105*, 19,095–19,109, 2000.

Rubin, A. M., D. Gillard, and J.-L. Got, Streaks of microearthquakes along creeping faults, *Nature*, *400*, 635–641, 1999.

Shaw, J. H., and P. M. Shearer, An elusive blind-thrust fault beneath metropolitan Los Angeles, *Science*, *283*, 1516–1518, 1999.

Shaw, J. H., and J. Suppe, Earthquake hazards of active blind-thrust faults under the central Los Angeles basin, California, *J. Geophys. Res.*, *101*, 8623–8642, 1996.

Shearer, P. M., Improving local earthquake locations using the L1 norm and waveform cross-correlation: Application to the Whittier Narrows, California, aftershock sequence, *J. Geophys. Res.*, *102*, 8269–8283, 1997.

Shearer, P. M., Evidence from a cluster of small earthquakes for a fault at 18 km depth beneath Oak Ridge, southern California, *Bull. Seismol. Soc. Am.*, *88*, 1327–1336, 1998.

Song, X. J., and D. V. Helmberger, Northridge aftershocks, a source study with TERRAscope data, *Bull. Seismol. Soc. Am.*, *87*, 1024–1034, 1997.

Thio, H. K., and H. Kanamori, Source complexity of the 1994 Northridge earthquake and its relation to aftershock mechanisms, *Bull. Seismol. Soc. Am.*, *86*, S84–S92, 1996.

Unruh, J. R., R. J. Twiss, and E. Hauksson, Kinematics of postseismic relaxation from aftershock focal mechanisms of the 1994 Northridge, California, earthquake, *J. Geophys. Res.*, *102*, 24,589–24,603, 1997.

Venkataraman, A., J. Mori, H. Kanamori, and L. Zhu, Fine structure of the rupture zone of the April 26 and 27, 1997, Northridge aftershocks, *J. Geophys. Res.*, *105*, 19,085–19,093, 2000.

Wald, D. J., T. H. Heaton, and K. W. Hudnut, The slip history of the 1994 Northridge, California, earthquake determined from strong-motion, teleseismic, GPS, and leveling data, *Bull. Seismol. Soc. Am.*, *86*, S49–S70, 1996.

Waldhauser, F., and W. L. Ellsworth, A double-difference earthquake location algorithm: Method and application to the northern Hayward fault, California, *Bull. Seismol. Soc. Am.*, *90*, 1353–1368, 2000.

Waldhauser, F., W. L. Ellsworth, and A. Cole, Slip-parallel seismic lineations on the northern Hayward fault, California, *Geophys. Res. Lett.*, *26*, 3525–3528, 1999.

Webb, T. H., and H. Kanamori, Earthquake focal mechanisms in the Eastern Transverse Ranges and San Emigdio Mountains, Southern California and evidence for a regional decollement, *Bull. Seismol. Soc. Am.*, *75*, 737–757, 1985.

Xie, J., Z. Liu, R. B. Herrmann, and E. Cranswick, Source processes of three aftershocks of the 1983 Goodnow, New York, earthquake: High resolution images of small symmetric ruptures, *Bull. Seismol. Soc. Am.*, *81*, 818–843, 1991.

Yeats, R. S., Late Cenozoic structure of the Santa Susana fault zone, *U.S. Geol. Surv. Prof. Pap.*, *1339*, 137–160, 1987.

Yeats, R. S., G. J. Huftile, and L. T. Stitt, Late Cenozoic tectonics of the east Ventura basin, Transverse Ranges, *AAPG Bull.*, *78*(7), 1040–1074, 1994.

Zhou, D., and H. Kanamori, The 1994 Northridge earthquake: 3-D crustal structure in the rupture zone and its relation to the aftershock locations and mechanisms, *Geophys Res. Lett.*, *22*, 763–766, 1995.

Zhou, D., H. Kanamori, and D. Wiens, State of stress before and after the 1994 Northridge earthquake, *Geophys. Res. Lett.*, *24*, 519–522, 1997.

L. Astiz, Vienna International Center, P.O. Box 1250, A-1400 Vienna, Austria. (Luciana.Astiz@ctbto.org)

J. L. Hardebeck and P. M. Shearer, Institute of Geophysics and Planetary Physics, University of California, San Diego, La Jolla, CA 92093-0225, USA. (jeanne@mahi.ucsd.edu; pshearer@ucsd.edu)

K. B. Richards-Dinger, Geothermal Program Office, NAWS, Code 83G000D, China Lake, CA 93555-6001, USA. (Richards-DingerKB@navair.navy.mil)